HHS Public Access

Author manuscript

Dent Mater. Author manuscript; available in PMC 2019 February 01.

Published in final edited form as:

Dent Mater. 2018 February ; 34(2): 209–220. doi:10.1016/j.dental.2017.10.001.

Collagenous matrix supported by a 3D-printed scaffold for osteogenic differentiation of dental pulp cells

Farahnaz Fahimipour[a,+], **Erfan Dashtimoghadam**[a,+], **Morteza Rasoulianboroujeni**[a], **Mostafa Yazdimamaghani**[b], **Kimia Khoshroo**[a], **Amir Yadegari**[a], **Mohammadreza Tahriri**[a], **Jose A. Gonzalez**[a], **Daryoosh Vashaee**[c], **Douglas C. Lobner**[d], **Tahereh S Jafarzadeh Kashi**[e], and **Lobat Tayebi**[a,f]

[a]Marquette University School of Dentistry, Milwaukee, WI 53233, USA

[b]School of Chemical Engineering, Oklahoma State University, Stillwater, OK 74078, USA

[c]Electrical and Computer Engineering Department, North Carolina State University, Raleigh, NC 27606, USA

[d]Department of Biomedical Sciences, Marquette University, Milwaukee, WI 53233, USA

[e]Dental Biomaterials Department, School of Dentistry, Tehran University of Medical Sciences, Tehran, Iran

[f]Department of Engineering Science, University of Oxford, Oxford OX1 3PJ, UK

Abstract

A systematic characterization of hybrid scaffolds fabricated based on combinatorial additive manufacturing technique and freeze-drying method are presented as a new platform for osteoblastic differentiation of dental pulp cells (DPCs). The scaffolds were consisted of a collagenous matrix embedded in a 3D-printed beta-tricalcium phosphate (β-TCP) as the mineral phase. The presented construct design was intended to achieve mechanical robustness owing to 3D-printed β-TCP scaffold, and biologically active 3D cell culture matrix pertaining to the collagen extracellular matrix. The β-TCP precursor formulations were investigated for their flow-ability at various temperatures to be optimized for fabrication of 3D printed scaffolds with interconnected porosity. The developed constructs were characterized by 3D laser scanning microscopy, X-ray diffraction, Fourier transform infrared spectroscopy, and compressive strength testing. The *in vitro* characterization of scaffolds revealed that the hybrid β-TCP/Collagen constructs offer superior DPCs proliferation and alkaline phosphatase (ALP) activity compared to the 3D-printed β-TCP scaffold over three weeks. Moreover, it was found that the incorporation of TCP into the collagen matrix improves the ALP activity. The obtained results converge to suggest the developed 3D-printed β-TCP/Collagen hybrid constructs as a new platform for osteoblastic differentiation of DPCs for craniomaxillofacial bone regeneration.

Correspondence to: Tahereh S Jafarzadeh Kashi; Lobat Tayebi.

[+]These authors contributed equally in this work.

Keywords

Collagen; β-TCP; 3D-printing; Hybrid scaffolds; Dental pulp cells; Osteogenic Differentiation

1. Introduction

Spontaneous regeneration capacity of bone tissue is only limited to small defects. Large bone defects as consequence of trauma, osteoporotic fracture, tumors, and congenital deformity require surgical intervention (Tare et al. 2010). Allografts and autografts are the main clinical strategies to fill bone cavities. However, autografts are restricted by site morbidity and approachability of the transplantable bone. Also, allografts increase the risk of immune-rejection reactions and infectious diseases transmission (Kurien et al. 2013). To address orthopedic challenges which results in reduced quality of life and patient discomfort, synthetic graft substitutes and implants have attracted tremendous interest in the last decade (Pina et al. 2015). An ideal synthetic bone graft should satisfy a number of optimized properties such as biodegradability, osteoconductivity, biocompatibility, interconnected porosity, and adequate mechanical strength (Bose et al. 2017) in order to fulfill vascularization, nutrient delivery, cellular attachment, proliferation, differentiation, integration into surrounding tissue, to be ultimately replaced with the *de novo* bone tissue (Khojasteh et al. 2016a).

An ideal scaffold for bone tissue engineering application should mimic natural bone properties such as morphology, porosity, composition, and mechanical strength (Razavi et al. 2015). Naturally, bone is composed of hydroxyapatite ($Ca_{10}(PO_4)_6(OH)_2$) in the context of organic matrix which is mainly comprised of collagen type I (Karageorgiou and Kaplan 2005). Different bone regions possess specific microstructure and function. Proximal tibial trabecular bone has typically pore size of 1 mm in diameter, 50–90% porosity, 0.30±0.10 g/cm^3 apparent density, 5.3 MPa ultimate strength, and 445 MPa elastic modulus. In contrast, femoral cortical bone is compact with limited voids, 3–12% porosity, 1.85±0.06 g/cm^3 apparent density, 193 MPa ultimate strength, and 17 GPa modulus of elasticity (Karageorgiou and Kaplan 2005). Bone is also a dynamic milieu, constantly repairing and remodelling its matrix by osteoblasts to create new mineralized bone matrix, ostoclasts disassembling and digesting the matrix, while the star-shaped osteocytes maintaining the matrix (Marks and Odgren 2002). Inspired by the hierarchical structure of the bone, the designed scaffolds for bone regeneration should structurally mimic the complexity of defected site and fulfill a 3D environment for initial cell attachment, consequent cell proliferation and tissue formation to ensure fixation and integration of scaffold with the host tissue (Hasani-Sadrabadi et al. 2015; Leukers et al. 2005). Generally, it has been suggested that fabrication of scaffolds with interconnected pores size over 300μm can facilitate cell attachment and migration, vascularization, mechanical interlocking, and tissue ingrowth (Khojasteh et al. 2016b).

There have been several fabrication techniques utilized to manufacture porous scaffold, including phase separation, salt leaching, freeze-drying, gas foaming, particle sintering, and solid free-form fabrication (SFF) techniques (Kim et al. 2006). Conventional non-SFF

approaches such as freeze-drying are limited in providing control on pore size, shape, interconnectivity, and construction of complex architectures (Fahimipour et al. 2016). Furthermore, the low compressive moduli of these scaffolds hamper their application for the load bearing bone regeneration. Over the past few years, SFF techniques have gained extreme attention which the major sub-groups of this approach are selective laser sintering and 3D-printing (Fahimipour et al. 2016). Additive layer manufacturing (ALM) or 3D-printing techniques offer the advantage of creating desired levels of complexity in custom made implants according to the medical requirements (Cox et al. 2015). In fact, 3D-printing method could be utilized in personalized medication level by obtaining individual patient computed tomography scan or magnetic resonance images (Dashtimoghadam et al. 2016). Indeed, 3D-printing is known as a reproducible and consistent technique. The major advantages and disadvantages of different classification of ALM techniques for bone tissue engineering applications have been thoroughly summarized elsewhere (Bose et al. 2013).

3D-printing technique enables fabrication of well-defined complex architectures both in micro and macro scales with improved mechanical properties, tuneable for different application such as soft or hard tissues (Sherwood et al. 2002). In spite of several advantages, 3D-printing suffers from the lack of ability to mimic nano-fibrous structure of extracellular matrix (ECM) which mainly supports cell adhesion, proliferation, communication, and differentiation. The advantages and disadvantages of conventional non-ALM approaches and 3D-printing, have motivated researches to exploit combinatorial fabrication techniques in order to better mimic the nature of bone tissue (Gross et al. 2014).

The motivation of the present work is to fabricate 3D-printed β-tricalcium phosphates (β-TCP) porous scaffolds which their pores were filled with freeze-dried collagen matrix. Hybridizing the 3D-printed β-TCP scaffold with freeze-dried collagen matrix would endow complementary properties, mechanical function supported by the ceramic scaffold and tissue regeneration owing to the collagenous matrix (Park et al. 2017; Zhang et al. 2017). The β-TCP was selected due to its chemical likeness to the bone mineral, which is commonly used in bone replacement applications (Liao et al. 2016). The physicomechanical and biological features of the developed β-TCP/Collagen hybrid constructs were completely investigated. The presented results here suggest that the combination of 3D-printing technique with freeze-drying method can provide optimal platforms to exploit osteogenic capacity of DPCs toward craniomaxillofacial bone regeneration.

2. Materials and Methods

2.1. Ink preparation and optimization

The paste formulations were composed of water, beta-tricalcium phosphate powder (β-TCP, Sigma), sodium tripolyphospahte (TPP, Alfa Aesar), and carboxymethylcellulose (CMC, Alfa Aesar). The TCP-based formulations were composed of 15 g TCP powder, 0.5 g TPP, 75 mg CMC, and 5.25, 5.75, and 7.75 ml water, which denoted as formulation 1, 2, and 3. The ink formulations were characterized to optimize their flow-ability for the 3D-printing process. Rheological measurements were performed by a rheometer (Kinexus, Malvern) using a cone-plate geometry. Shear stress and viscosity were measured altering formulations temperature from 17 to 29 °C, and shear rate of 0–100 1/s.

2.2. Fabrication of β-TCP scaffolds using 3D-printing technique

3D-Bioplotting system (Envisiontec, Germany) was utilized to fabricate scaffolds with desired geometry, size, and structure. A CAD/CAM software was used to design disk block models of scaffold. The 3D-printing was performed on paste formulations at 5 mm/s dispensing speed, optimal pressure of 1.5 bar, and a plotting needle (Nordson, USA) owning an inner diameter of 400um to obtain 0.6–0.8 mm distanced strands with 90 degree shifted between layers. Disc of 15 mm diameter and 2 mm thickness were prepared in a layer-by-layer deposition of strands from the printer head. The fabricated scaffolds were air dried overnight, and sintered in controlled high temperature muffle furnace (MTI, USA). A sequential temperature profile was used for sintering the 3D-printed scaffolds as follows: heating up uniformly to 600 °C at 3°C/min, incubation for 1 hour at 600 °C, heating up from 600 to 1100 °C at 5°C/min, and incubation at 1100 °C for 4 hours

2.3. X-ray diffraction analysis

X-ray diffraction (XRD) was carried out to characterize the TCP powder and scaffold. Sintered scaffolds were ground using an agate mortar and pestle. The powder was then sieved to 150 μm particles.

2.4. Isolation and characterization of rat tail Collagen type I

Collagen type I was extracted from Wistar rat tail based on a protocol described elsewhere (Rajan et al. 2006). In brief, bone and tendons were exposed and removed by folding the tails. After washing with PBS, tendons were dissolved in 0.1 M autoclaved acetic acid at 4°C for 7 days. Collagen foam was then obtained by freeze-drying the solution. A stock solution with 5 mg/ml concentration was prepared by re-dissolving the collagen foam in 0.1 M acetic acid aqueous solution, and stored at 4°C for further usage.

2.5. Differential scanning calorimetry

Differential scanning calorimetry technique (DSC, NETZCH) was employed with scan rate of 10 °C/min to identify the extracted collagen denaturation temperature. The freeze-dried extracted collagen samples were characterized through two methods, one was direct heating up from the room temperature, and the other was heating up from room temperature to 130°C, isothermal incubation for 1 h, and heating up to 250°C to eliminate the effect of residual hydration.

2.6. Fabrication of β-TCP/Col hybrid constructs

The prepared collagen solution ($5 mg.ml^{-1}$) described above in pure state or mixed with β-TCP powder (50 *wt*% of the dry weight of collagen) was filled into pores of the 3D-printed β-TCP scaffolds, and then frozen by 10 min immersion in liquid nitrogen. Subsequently, the frozen mixture was lyophilized to produce β-TCP/Collagen hybrid construct. The collagen-based matrices formed inside the scaffold pores were further crosslinked using 1-(3-dimethylaminopropyl)-3-ethylcarbodiimide hydrochloride (EDC, TCI Chemicals) and hydroxysuccinimide (NHS, Alfa Aesar) to increase their stability. The constructs were denoted as β-TCP/Col and β-TCP/Col-TCP.

2.7. Morphological characterization of β-TCP scaffolds and β-TCP/Col hybrid constructs

The microstructure and morphology of the β-TCP scaffolds and β-TCP/Col hybrid constructs were assessed by a 3D laser scanning digital microscope (Olympus LEXT OLS 4000, Japan). At least 3 different sites of 3D-printed scaffolds and hybrid constructs were randomly selected to measure the dimensions of the pore size, thickness of strands, distance between strands, and other microstructural features using the image software (LEXT OLS 4000).

2.8. Fourier transform infrared spectroscopy

Fourier-transform infrared (FT-IR) spectroscopy (Nicolet iS5 Thermo Scientific™ USA, OMNIC™) was performed to identify the functional vibrations groups in the fabricated constructs over the range of 4000–600 cm^{-1} wavenumber at a resolution of 4 cm^{-1}.

2.9. Porosity and mechanical properties

Porosity was measured using solvent displacement method as previously reported (Shahini et al. 2014). Briefly, scaffolds were weighed in dry state and then immersed in 10 ml ethanol. The specimens containing ethanol were weighed and porosity of scaffolds was calculated using the following equation:

$$Porosity = \frac{(W_w - W_d) \times 100\,\%}{\rho \times \pi R^2 T}$$

where W_w and W_d are the weight of scaffold in wet and dry state, ρ is the solvent density, and R, T are the radius and thickness of scaffolds, respectively.

The compressive modulus and strength of the collagen-based matrices and β-TCP/Col constructs were measured utilizing a mechanical testing machine (Shimadzu, Japan) with cross-head speed of 1.0 $mm.min^{-1}$ and a 5kN load cell. The cylindrical samples (n=5) were compressed until they crushed. Furthermore, the compressive modulus of the 3D-printed β-TCP scaffolds after immersion in PBS was measure over 4 weeks.

2.10. Isolation and characterization of dental pulp stem cells

Dental pulp stem cells from the pulp tissue were isolated to study cell attachment, proliferation, and differentiation on the fabricated scaffolds and constructs. According to a protocol reported elsewhere, normal impacted third molars were washed several times with PBS containing 100 mg/ml streptomycin and 100 U/ml penicillin. Pulp tissues were removed, transferred to sterile dish and then cut into small pieces. An enzyme solution consisted of 4 mg/ml dispase (Sigma), and 3 mg/ml type I collagenase (Sigma) in Hank's Balanced Salt Solution (HBSS, Sigma) were used to digest the pulp tissue for 1h at 37°C with a regular agitation. The digest was added to 5 ml of alpha-minimal essential medium (αMEM, Sigma) supplemented with 15% FBS (Sigma), and centrifuged at 300 g for 5 minutes. Afterward, the products were centrifuged and pellet was suspended in fresh αMEM supplemented with 15% FBS. The isolated dental pulp stem cells (DPSCs) were then

cultured into tissue culture polystyrene (TCPS) and incubated at 5% CO_2 and 37°C for further experiments.

Alizarin red assay was applied to confirm osteogenic capability of DPSCs. In brief, the extracted DPSCs at passage three were cultured on TCPS for 3 weeks in osteogenic medium, consisting of αMEM supplemented with 10% FBS, 50 μg/ml ascorbic acid, 10 mM β-glycerophosphate and 10 nM dexamethasone and then fixed, washed and stained with alizarin red staining solution (Alfa Aesar). The DPCs were also characterized for their cell-surface markers expression by fluorescence activated cell sorting (FACS) technique (Attune® Acoustic Focusing Cytometer, Thermo Fisher Scientific)

2.11. Cell adhesion

Scanning Electron Microscopy (SEM) was performed on cells attached on the scaffolds to study morphology of cells on scaffolds. To do this, scaffolds were removed from the culture medium, washed in PBS, and fixed with 4% of glutaraldehyde. Cells were dehydrated in gradient ethanol concentrations of 50, 70, 80, 90 and 100% to conserve their intact morphology. Images were then captured using a scanning electron microscope (JEOL-JSM6510).

2.12. Cell proliferation

PrestoBlue® (PB) cell vitality assay (Invitrogen, USA) was carried out according to the manufacturer's instructions at different time intervals of 7, 14 and 21 days after cell culture. Cells were seeded on 12 well-plates and media were changed every other day. The fluorescence measurements (Ex: 560 nm and Em: 590 nm) were determined by a spectrophotometric plate reader (Synergy HTX, BioTEK).

2.13. Cell differentiation

Alkaline phosphatase (ALP) activity of DPCs cultured on scaffolds was implemented utilizing an ALP assay kit (Abcam, USA). The samples were incubated in osteogenic medium and tested after 7, 14 and 21 days to investigate osteogenic differentiation of DPCs. The lysates obtained from DPCs digestion were reacted with p-nitrophenyl phosphate (p-NPP), and the absorbance of p-nitrophenol was measured at 405 nm employing a microplate reader (Synergy HTX, BioTEK) to indicate the ALP quantity.

2.14. Statistical analysis

All data were expressed as mean ± standard deviation (Mean ±SD). The significance difference was calculated by one-way ANOVA complemented by Tukey's multiple comparisons test. *P*-values <0.05 were considered to be statistically significant.

3. Results

In order to obtain a β-TCP-based paste formulation with appropriate flowability to be used in the 3D-printing process, their rheological features including shear stress and shear viscosity were studied at various temperatures. Shear stress as a function of shear rate for the paste formulations is shown in Figure 1A–C, which indicates a Bingham pseudoplastic

behavior for the paste formulations. All formulations were found to show a yield stress, which is required for the 3D-printing process. As can be seen in Figure 1D–F, the highly β-TCP filled paste inks exhibits shear-thinning behavior as shear viscosity decreases with increasing shear rate. It was found that with increasing water content in paste formulations shear viscosity decreases indicating the augmentation of flowability of the paste formulations. Based on the obtained results, the formulation 2 was selected for 3D-printing process, which was found to fulfill reliable dispensing at pressure of 1.5 bar while maintaining the strand shape. In other words, formulation 2 was figured out to have the minimum amount of water to provide aforementioned paste features for the 3D-printing process. It is worthy of note that the formulation 2 showed the lowest dependence on temperature alteration, which helps additive layer manufacturing of the β-TCP scaffolds in a reproducible manner.

The X-ray diffraction (XRD) patterns of two TCP samples are demonstrated in Figure 2A as received powder and ground sintered 3D-printed TCP scaffolds. As can be seen, both samples show the characteristic peaks of the primarily β-TCP phase (Xue et al. 2009).

The isolated Collagen (Col) was characterized through differential scanning calorimetry (DSC) at fully dried and partially hydrated states. The DSC thermograms are shown in Figure 2B, where the distinctive peaks are attributed to the denaturation of the collagen chains. In order to eliminate the plasticizing effect of residual water on denaturation, the freeze-dried collagen sample went through the following heating steps: heating up from room temperature to 130°C, isothermal incubation for 1 h, and finally heating up to 250°C. As can be seen in Figure 2B, the onset and peak temperatures were measured to be about 193.7 and 203.9°C, respectively. In order to evaluate the collagen matrix comprising structural residual water, the freeze-dried samples were heated up without isothermal step. In this way, the onset and peak temperatures were obtained as 102.5 and 113.1°C, respectively (see the inset shown in Figure 2B).

Figure 2C shows the FT-IR spectra of collagen, β-TCP, and Collagen-TCP composite matrix. As seen, the C=O stretching of carboxamide (amid I) functional groups along the polypeptide backbone observed at 1653 cm^{-1}. The distinctive peaks observed at 1546 and 1234 cm^{-1} are related to N-H bending vibrations and C-H stretching of amide II and III bands, respectively. In addition, stretching of N-H groups coupled with hydrogen bonding (amid A) and amid B bonding (C-H stretching) at broad band ranging from 3200 to 3600 cm^{-1} is ascribed to the collagen characteristic peak (Payne and Veis 1988). The spectrum of β-TCP exhibited the characteristic spectral bands at 1119, 1079, 1027, 976 and 947 cm^{-1} attributed to vibrational mode of ${}_3PO_4^{3-}$ (Moreira et al. 2014). As can be seen, both characteristics peaks of the collagen and β-TCP are observed in the FT-IR spectrum of Collagen-TCP composite sample.

The schematic representation of the developed combinatorial approach to fabricate hybrid constructs consisted of freeze-dried collagen matrix supported by 3D-printed β-TCP scaffold are shown in Figure 3A. The presented methodology offers combined advantages of the 3D porous ECM-like collagen matrix for cell growth and proliferation, supported by 3D printed β-TCP scaffold. The macro- to microscale structural features of 3D-printed β-TCP scaffold

as well as 3D-printed β-TCP/Col hybrid constructs are shown in Figure 3B–D and 3E–G, respectively. As seen in Figure 3B–D, the optimized paste formulation 2 has allowed to obtain precise printing of β-TCP scaffolds, acquiring mechanical function of the hybrid constructs. As observed in Figure 3E–G, the hybrid construct is mainly composed of a freeze-dried collagen matrix with interconnected porosity inside the pores of 3D-scaffold to provide a platform for cell attachment and growth.

The 3D laser scanning micrographs of the 3D-printed β-TCP scaffold is shown in Figure 4A. As can be seen, the pore size of the scaffolds was found to be in the range of 426±17 μm. As evident in Figure 4B, biodegradation of scaffolds have resulted in decreased compressive modulus over time, which was found to become more pronounced after 2 and 4 weeks. However, it should be noted that after four weeks of immersion, scaffold still maintain over 30% of their initial compressive modulus providing host tissue enough time for ingrowth into the constructs.

The porosity of Collagen and Collagen-TCP matrices were compared with β-TCP/Col and β-TCP/Col-TCP hybrid constructs in Figure 4C. As displayed, the porosity of Collagen and Collagen-TCP matrices is reduced from 97.7±0.4% and 97.2±0.3% to 42.1±0.9% and 42.2±3.1% after incoporation into the 3D-printed β-TCP scaffold.

The compressive modulus of Collagen and Collagen-TCP matrices were compared with β-TCP/Col and β-TCP/Col-TCP hybrid constructs in Figure 4D.

As shown in Figure 4E, F, the extracted DPCs have formed fibroblast-like morphology. The osteogenic differentiation of DPCs was confirmed with the positive Alizarin Red S staining shown in Figure 4G. DPCs were also investigated for their surface markers. Figure 4H shows the immunofluorescence images of 2D cultured DPCs using positive surface marker CD90 and DAPI.

Hematoxylin and eosin (H&E) staining of cultured DPCs onto 3D-printed β-TCP/Col-TCP construct after three weeks was shown in Figure 5A. As can be seen, the DPCs were attached and well proliferated onto the construct. This observation implies the interconnected porosity in constructs has allowed for the flux of nutrition inside the scaffold and removal of waste produced by the cells. As described above, the β-TCP/Col heterophasic constructs were designed to mimic the native bone ECM and endow a 3D microenvironment for DPCs. Figure 5B–C and Figure 5D–E show the scanning electron micrographs for 3D-printed β-TCP scaffold, and 3D-printed β-TCP/Col-TCP construct seeded with DPCs after three weeks, respectively. As can be seen, the incorporation of the freeze-dried Col matrix into the β-TCP scaffold resulted in considerably improved attachment and proliferation of DPCs, which implies the enhanced seeding efficiency onto the hybrid constructs.

The immunofluorescent images of cultured DPCs onto β-TCP/Col and β-TCP/Col-TCP constructs after 3 weeks are displayed in Figure 5F–G. As evident, the DPCs proliferated more onto the β-TCP/Col than β-TCP/Col-TCP construct. In order to get a quantitative insight into cells proliferation, the viability of DPCs cultured onto the 3D-printed β-TCP scaffold was compared with β-TCP/Col and β-TCP/Col-TCP constructs over three weeks.

Figure 5H demonstrate significantly improved proliferation of DPCs cultured onto the β-TCP/Col and β-TCP/Col-TCP hybrid constructs compared with the β-TCP scaffold. As can be seen in Figure 5I, the increased ALP expression indicates that cells underwent differentiation and induced osteogenic markers. Similarly for 3D-printed β-TCP scaffold, as well as β-TCP/Col and β-TCP/Col-TCP constructs a time dependant increase of DPCs differentiation was observed. The ALP activity of DPCs cultured onto the β-TCP/Col-TCP was found to be significantly higher than the other groups.

Discussion

The flowability of designed β-TCP-based ink formulations was optimized for the 3D-printing process. According to the formulations described in the method section, the β-TCP-based paste inks were composed of constant amount of β-TCP, carboxymethylcellulose (CMC) and sodium tripolyphospahte (TPP), but different volume of water. In the presented ink formulations CMC and TPP act as the binder and viscosity modifier, respectively; while various amounts of water were intended to tune the flow-ability of the paste and merging of strands during 3D-printing process. The shear sweep measurements revealed a yield stress and a shear-thinning behaviour for the paste formulations, which were found to be necessary for the 3D-printing process. The shear viscosity results at various temperatures from 17°C to 26°C indicated the reduction of shear viscosity with increasing temperature. This observation is closely related to the screening of hydrogen bonds among binder CMC chains, which facilitates the flow-ability of the paste ink.

The quality of the isolated collagen was verified by the differential scanning calorimetry (DSC) method through assessment of its denaturation behaviour. Collagen chains undergo denaturation due to breaking of various intermolecular interactions including disulfide bonds, glycosylation of lysine and hydroxylysine residues (Miles and Bailey 1999; Robins and Bailey 1975). It has been shown that water residue plays a substantial role in thermal stability of collagen fibres, in which dehydration considerably upsurges thermal denaturation of the collagen fibrillar network (Miles and Burjanadze 2001; Miles et al. 2005). By increasing temperature, the intramolecular hydrogen bonds stabilizing collagen chains are disappeared; hence, the triple helix structures collapse (Fraser et al. 1979; Miles et al. 1995).

Inspired by the native bone extracellular matrix, which is composed of the mineral phase embedded into a mainly collagenous network, TCP was incorporated into freeze-dried collagen matrix in order to improve the osteogenic potential of the designed heterophasic constructs. It is worth to note that the inclusion effect of β-TCP added into the collagen matrix on the porosity was not significant. This indicates marginal influence of β-TCP on pore formation in collagen matrix by freeze-drying method. The porosity of the β-TCP/Col constructs resembles proximal tibial trabecular bone, which has typically 50–90% porosity (FU 2010).

As expected, a drastic difference in compressive modulus of freeze-dried collagen-based matrices and the hybrid constructs was observed. It was found that the compressive modulus of freeze-dried collagen-based matrices increases to more than 3 orders of magnitude after inclusion into the 3D-printed β-TCP scaffolds. In order to get an insight into the fate of 3D-

printed β-TCP scaffolds responsible for the mechanical function of the hybrid constructs, their compressive modulus over 4 weeks immersion in PBS was compared with the dry state. The 3D-printed β-TCP scaffolds were found to preserve more than 30% of their initial compressive modulus, which allows for ingrowth of the cells into the constructs and gradual replacement of the regenerated bone tissue.

Isolation of human dental pulp stem cells (DPSCs) as an odontogenic progenitor from impacted adult dental pulp tissue was first reported by Gronthos *et al* in 2000 (Gronthos et al. 2000). Over the past years, DPSCs have shown great capacity for bone regeneration owing to their potential to provide osteoinductive bone factors and differentiation to osteoblasts *in vitro* and *in vivo* (Seong et al. 2010). The extracted DPSCs have formed fibroblast-like morphology, as reported by other researchers (Gronthos et al. 2000). DPSCs have both several similarities and differences to bone marrow stromal cells (BMSCs) (Tatullo et al. 2015). DPSCs have significantly higher colony-forming ability and number of proliferating cells compared to BMSCs over similar plating densities (Gronthos et al. 2000). After three weeks osteogenic differentiation, Alizarin Red S staining, as a functional assay, was performed on cultured DPSCs to assess their differentiation capacity. Kawashima has discussed the typical surface markers of DPSCs, and defined them to be positive for CD44, CD73, CD90 and CD105, while they are negative towards haematopoietic markers of CD34, CD45, and HLA-DR (Kawashima 2012). In consistent with these features, the presented results from the fluorescence activated cell sorting analysis of DPCs converge to indicate the successful DPSCs isolation.

It was found that the hybrid constructs offer drastically improved cell viability compared to the pristine β-TCP scaffold. Such capability originates from the implemented combinatorial fabrication technique through inclusion of the freeze-dried collagen matrix into the 3D-printed mineral support. Although no significant difference was observed between the β-TCP/Col and β-TCP/Col-TCP in the term of cell viability over the first week, but β-TCP/Col-TCP showed superior proliferation after two and three weeks post culture time. Such an improvement could be associated with the incorporation of β-TCP phase into the collagen matrix.

Alkaline phosphatase (ALP) is an early osteogenic differentiation marker and also an ectoenzyme elaborating degradation of inorganic pyrophosphate involved in release of phosphate for bone mineralization (Stucki et al. 2001). In order to assess the designed constructs as osteogenic platform for DPCs, their (ALP) activity of was measured over three weeks. The increased ALP expression indicates that cells underwent differentiation and induced osteogenic markers. Similarly for 3D-printed β-TCP scaffold, as well as β-TCP/Col and β-TCP/Col-TCP constructs a time dependant increase of DPCs differentiation was observed. The ALP activity of DPCs cultured onto β-TCP/Col-TCP was found to be significantly higher than other groups. Such effect resembles the osteogenic differentiation of hMSCs promoted by the CaP-rich mineral microenvironment in bone ECM *via* phosphate-ATP-adenosine metabolic signaling (PNAS, 111, 2014, 990–995). Indeed, the dynamic dissolution/precipitation CaP minerals govern the Ca^{2+} and PO_4^{3-} ions concentration in the ECM. It has been shown that cells uptake the PO_4^{3-} ions through the

solute carrier family 20 (phosphate transporter), member 1 (SLC20a1) and then enters the mitochondria for ATP synthesis. The secreted ATP is subsequently metabolized into adenosine, which promotes osteogenic differentiation of hMSCs. These results are in accordance with other reports (Ajlan et al. 2015; Khanna-Jain et al. 2012).

4. Conclusions

A major challenge in scaffold design for bone tissue engineering is to employ various fabrication techniques to achieve platforms with combined mechanical function and regenerative capacity. In this study, a combinatorial fabrication approach based on the successive employment of 3D-printing technique and freeze-drying method was developed to design heterophasic constructs for osteoblastic differentiation of dental pulp stem cells (DPSCs). Inspired by the anisotropic microstructure of the native bone tissues, the designed constructs were consisted of a 3D-printed β-TCP scaffold with interconnected porosity resembling the bone mineral phase to fulfill the mechanical function, embedded with a collagenous matrix to mimic the bone extracellular matrix and support DPCs adhesion, proliferation, and osteogenic differentiation. The obtained results demonstrated a great potential of the developed constructs for regeneration of craniomaxillofacial bone defects.

References

Ajlan SA, Ashri NY, Aldahmash AM, Alnbaheen MS. Osteogenic differentiation of dental pulp stem cells under the influence of three different materials. BMC oral health. 2015; 15(1):132. [PubMed: 26510991]

Bose S, Tarafder S, Bandyopadhyay A. Effect of chemistry on osteogenesis and angiogenesis towards bone tissue engineering using 3d printed scaffolds. Annals of biomedical engineering. 2017; 45(1): 261–272. [PubMed: 27287311]

Bose S, Vahabzadeh S, Bandyopadhyay A. Bone tissue engineering using 3d printing. Materials Today. 2013; 16(12):496–504.

Cox SC, Thornby JA, Gibbons GJ, Williams MA, Mallick KK. 3d printing of porous hydroxyapatite scaffolds intended for use in bone tissue engineering applications. Materials Science and Engineering: C. 2015; 47:237–247. [PubMed: 25492194]

Dashtimoghadam E, Fahimipour F, Davaji B, Hasani-Sadrabadi M, Tayebi L. Microfluidic-directed synthesis of polymeric nanoparticles for bone cancer therapy. Dental Materials. 2016; 32:e59–e60.

Fahimipour F, Kashi TJ, Khoshroo K, Dashtimoghadam E, Rasoulianborujeji M, Tayebi L. 3d-printed β-tcp/collagen scaffolds for bone tissue engineering. Dental Materials. 2016; 32:e57.

Fraser R, MacRae T, Suzuki E. Chain conformation in the collagen molecule. Journal of molecular biology. 1979; 129(3):463–481. [PubMed: 458854]

FUCLX. Development of a bioresorbable bone graft alternative for bone engineering applications. 2010

Gronthos S, Mankani M, Brahim J, Robey PG, Shi S. Postnatal human dental pulp stem cells (dpscs) in vitro and in vivo. Proceedings of the National Academy of Sciences. 2000; 97(25):13625–13630.

Gross BC, Erkal JL, Lockwood SY, Chen C, Spence DM. Evaluation of 3d printing and its potential impact on biotechnology and the chemical sciences. ACS Publications. 2014

Hasani-Sadrabadi MM, Hajrezaei SP, Emami SH, Bahlakeh G, Daneshmandi L, Dashtimoghadam E, Seyedjafari E, Jacob KI, Tayebi L. Enhanced osteogenic differentiation of stem cells via microfluidics synthesized nanoparticles. Nanomedicine: Nanotechnology, Biology and Medicine. 2015; 11(7):1809–1819.

Karageorgiou V, Kaplan D. Porosity of 3d biomaterial scaffolds and osteogenesis. Biomaterials. 2005; 26(27):5474–5491. [PubMed: 15860204]

Kawashima N. Characterisation of dental pulp stem cells: A new horizon for tissue regeneration? Archives of Oral Biology. 2012; 57(11):1439–1458. [PubMed: 22981360]

Khanna-Jain R, Mannerström B, Vuorinen A, Sándor GK, Suuronen R, Miettinen S. Osteogenic differentiation of human dental pulp stem cells on β-tricalcium phosphate/poly (l-lactic acid/caprolactone) three-dimensional scaffolds. Journal of tissue engineering. 2012; 3(1) 2041731412467998.

Khojasteh A, Fahimipour F, Eslaminejad MB, Jafarian M, Jahangir S, Bastami F, Tahriri M, Karkhaneh A, Tayebi L. Development of plga-coated β-tcp scaffolds containing vegf for bone tissue engineering. Materials Science and Engineering: C. 2016a; 69:780–788. [PubMed: 27612772]

Khojasteh A, Fahimipour F, Jafarian M, Sharifi D, Jahangir S, Khayyatan F, Baghaban Eslaminejad M. Bone engineering in dog mandible: Coculturing mesenchymal stem cells with endothelial progenitor cells in a composite scaffold containing vascular endothelial growth factor. Journal of Biomedical Materials Research Part B: Applied Biomaterials. 2016b

Kim S-S, Park MS, Jeon O, Choi CY, Kim B-S. Poly (lactide-co-glycolide)/hydroxyapatite composite scaffolds for bone tissue engineering. Biomaterials. 2006; 27(8):1399–1409. [PubMed: 16169074]

Kurien T, Pearson R, Scammell B. Bone graft substitutes currently available in orthopaedic practice. Bone Joint J. 2013; 95(5):583–597. [PubMed: 23632666]

Leukers B, Gülkan H, Irsen SH, Milz S, Tille C, Schieker M, Seitz H. Hydroxyapatite scaffolds for bone tissue engineering made by 3d printing. Journal of Materials Science: Materials in Medicine. 2005; 16(12):1121–1124. [PubMed: 16362210]

Liao HT, Lee MY, Tsai WW, Wang HC, Lu WC. Osteogenesis of adipose-derived stem cells on polycaprolactone–β-tricalcium phosphate scaffold fabricated via selective laser sintering and surface coating with collagen type i. Journal of Tissue Engineering and Regenerative Medicine. 2016; 10(10)

Marks SC, Odgren PR. Structure and development of the skeleton. Principles of bone biology. 2002; 1:3–15.

Miles C, Burjanadze T. Thermal stability of collagen fibers in ethylene glycol. Biophysical journal. 2001; 80(3):1480–1486. [PubMed: 11222308]

Miles CA, Avery NC, Rodin VV, Bailey AJ. The increase in denaturation temperature following cross-linking of collagen is caused by dehydration of the fibres. Journal of Molecular Biology. 2005; 346(2):551–556. [PubMed: 15670603]

Miles CA, Bailey AJ. Thermal denaturation of collagen revisited. Journal of Chemical Sciences. 1999; 111(1):71–80.

Miles CA, Burjanadze TV, Bailey AJ. The kinetics of the thermal denaturation of collagen in unrestrained rat tail tendon determined by differential scanning calorimetry. Journal of molecular biology. 1995; 245(4):437–446. [PubMed: 7837274]

Moreira APD, Sader MS, Soares GDdA, Leão MHMR. Strontium incorporation on microspheres of alginate/β-tricalcium phosphate as delivery matrices. Materials Research. 2014; 17(4):967–973.

Park J, Lee SJ, Jo HH, Lee JH, Kim WD, Lee JY, Su A. Fabrication and characterization of 3d-printed bone-like β-tricalcium phosphate/polycaprolactone scaffolds for dental tissue engineering. Journal of Industrial and Engineering Chemistry. 2017; 46:175–181.

Payne K, Veis A. Fourier transform ir spectroscopy of collagen and gelatin solutions: Deconvolution of the amide i band for conformational studies. Biopolymers. 1988; 27(11):1749–1760. [PubMed: 3233328]

Pina S, Oliveira JM, Reis RL. Natural-based nanocomposites for bone tissue engineering and regenerative medicine: A review. Advanced Materials. 2015; 27(7):1143–1169. [PubMed: 25580589]

Rajan N, Habermehl J, Coté M-F, Doillon CJ, Mantovani D. Preparation of ready-to-use, storable and reconstituted type i collagen from rat tail tendon for tissue engineering applications. Nature protocols. 2006; 1(6):2753. [PubMed: 17406532]

Razavi M, Fathi M, Savabi O, Vashaee D, Tayebi L. In vivo assessments of bioabsorbable az91 magnesium implants coated with nanostructured fluoridated hydroxyapatite by mao/epd technique

for biomedical applications. Materials Science and Engineering: C. 2015; 48:21–27. [PubMed: 25579892]

Robins SP, Bailey AJ. The chemistry of the collagen cross-links. The mechanism of stabilization of the reducible intermediate cross-links. Biochemical Journal. 1975; 149(2):381–385. [PubMed: 1237296]

Seong JM, Kim B-C, Park J-H, Kwon IK, Mantalaris A, Hwang Y-S. Stem cells in bone tissue engineering. Biomedical Materials. 2010; 5(6):062001. [PubMed: 20924139]

Shahini A, Yazdimamaghani M, Walker K, Eastman M, Hatami-Marbini H, Smith B, Ricci J, Madihally S, Vashaee D, Tayebi L. 3d conductive nanocomposite scaffold for bone tissue engineering. International Journal of Nanomedicine. 2014; 9:167– 181. [PubMed: 24399874]

Sherwood JK, Riley SL, Palazzolo R, Brown SC, Monkhouse DC, Coates M, Griffith LG, Landeen LK, Ratcliffe A. A three-dimensional osteochondral composite scaffold for articular cartilage repair. Biomaterials. 2002; 23(24):4739–4751. [PubMed: 12361612]

Stucki U, Schmid J, Hämmerle CF, Lang NP. Temporal and local appearance of alkaline phosphatase activity in early stages of guided bone regeneration. Clinical oral implants research. 2001; 12(2): 121–127. [PubMed: 11251661]

Tare R, Kanczler J, Aarvold A, Jones A, Dunlop D, Oreffo R, Tanner KE, Dalby MJ. Skeletal stem cells and bone regeneration: Translational strategies from bench to clinic. Proceedings of the Institution of Mechanical Engineers, Part H: Journal of Engineering in Medicine. 2010; 224(12): 1455–1470.

Tatullo M, Marrelli M, Shakesheff KM, White LJ. Dental pulp stem cells: Function, isolation and applications in regenerative medicine. Journal of tissue engineering and regenerative medicine. 2015; 9(11):1205–1216. [PubMed: 24850632]

Xue W, Bandyopadhyay A, Bose S. Polycaprolactone coated porous tricalcium phosphate scaffolds for controlled release of protein for tissue engineering. Journal of Biomedical Materials Research Part B: Applied Biomaterials. 2009; 91(2):831–838.

Zhang M-L, Cheng J, Xiao Y-C, Yin R-F, Feng X. Raloxifene microsphere-embedded collagen/chitosan/β-tricalcium phosphate scaffold for effective bone tissue engineering. International journal of pharmaceutics. 2017; 518(1):80–85. [PubMed: 27988379]

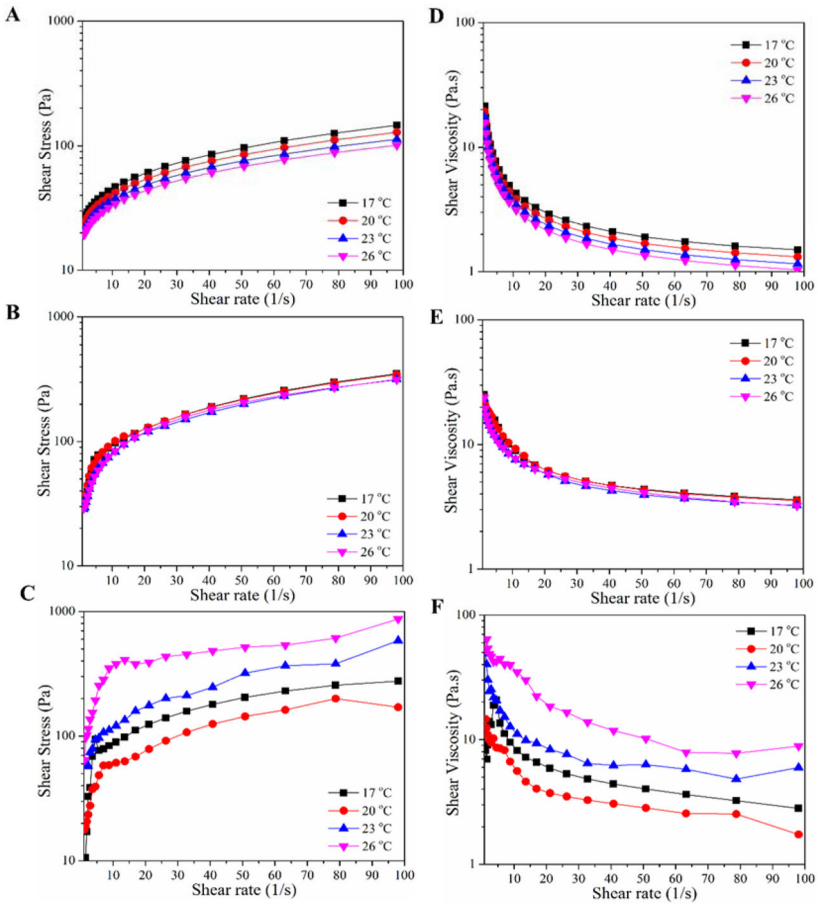

Figure 1.

(A–C) Shear stress as a function of shear rate at various temeartures for β-TCP-based paste formulations described in **Table 1** (**A**: formulation 1, **B**: formulation 2, and **C**: formulation 3). **(D–F)** Dependance of shear viscosity on shear rate at different temeartures for the β-TCP-based paste formulations (**D**: formulation 1, **E**: formulation 2, and **F**: formulation 3).

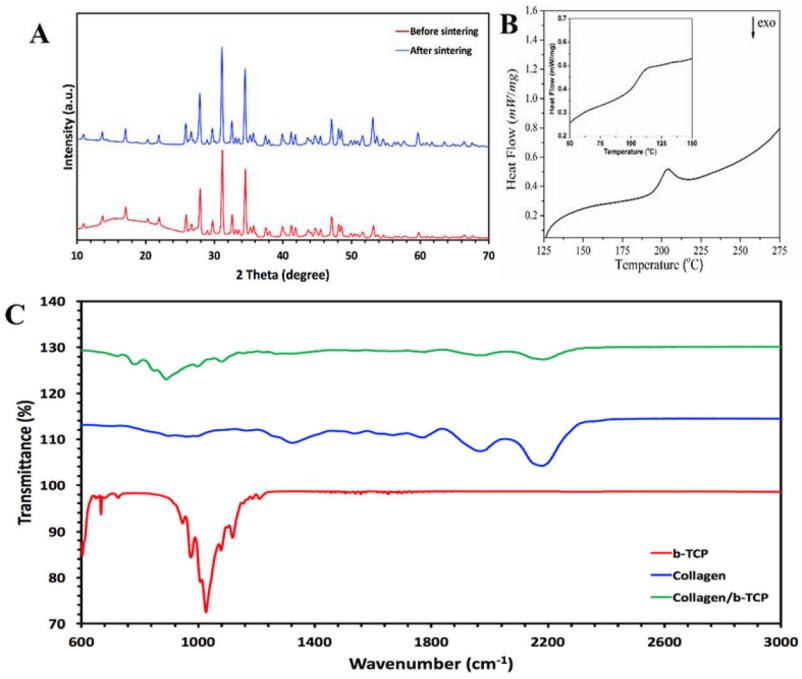

Figure 2.

(A) The X-ray diffraction patterns of TCP samples, as received β-TCP powder in comparison with the ground sintered 3D-printed TCP scaffolds (The inset shows a schematic representation of 3D-printed β-TCP-based scaffolds). **(B)** Differential scanning calorimetry (DSC) thermogram of fully dehydrated freeze-dried Collagen matrix (The inset displays the corresponding DSC thermogram for the freeze-dried Collagen matrix). **(C)** Fourier transform infrared spectra of β-TCP, Collagen, and Collagen-TCP composite samples.

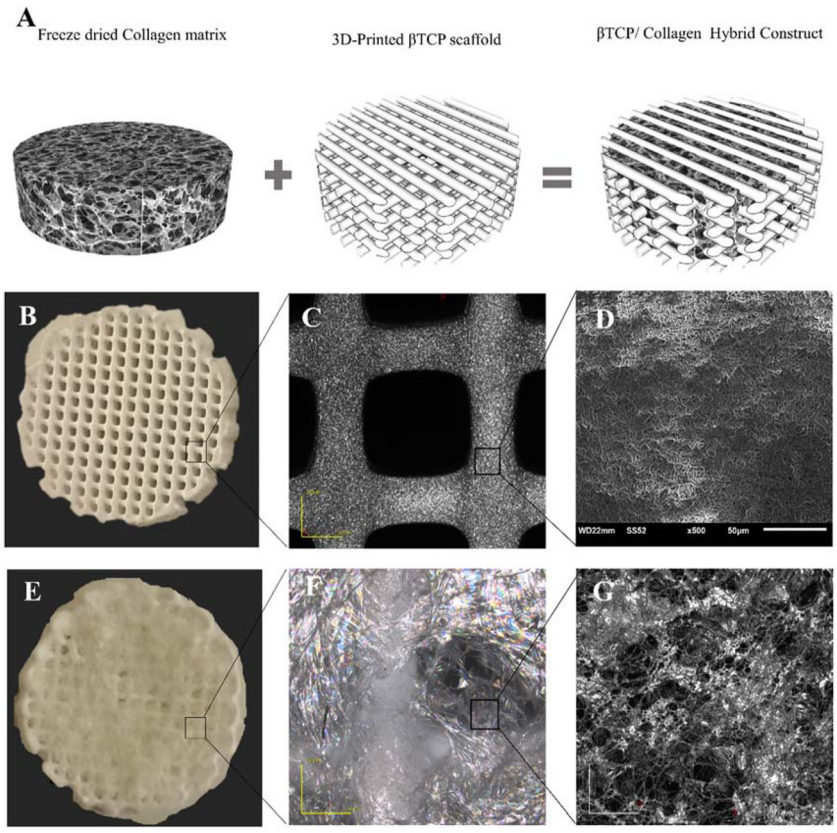

Figure 3.

(A) Schematic representation of the combinatorial approach developed to fabricate hybrid constructs consisted of freeze-dried collagen matrix supported by 3D-printed β-TCP scaffold. **(B–D)** Macro- to microscale demonstration of structural features of 3D-printed β-TCP scaffold. **(E–G)** Macro- to microscale demonstration of structural features of 3D-printed β-TCP/Col hybrid constructs.

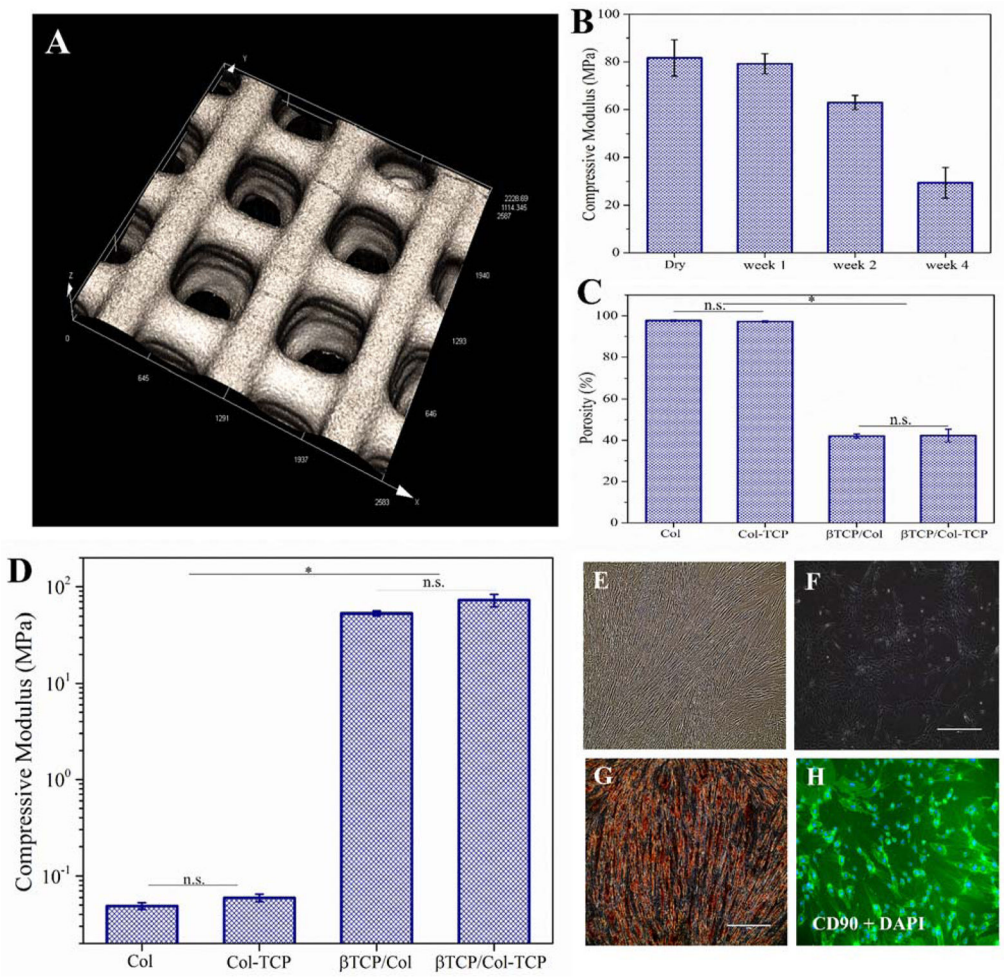

Figure 4.

(A) 3D laser scanning micrographs of the 3D-printed β-TCP scaffold (The scale bar is 500 μm). Porosity of Collagen and Collagen-TCP matrices compared with β-TCP/Col and β-TCP/Col-TCP hybrid constructs. **(C)** Compressive modulus of 3D-printed β-TCP scaffolds in dry state and after 1, 2, and 4 weeks immersion in phosphate-buffered saline. **(D)** Compressive modulus of Collagen and Collagen-β. TCP matrices compared with β-TCP/Col and β-TCP/Col-TCP hybrid constructs **(E,F)** optical image of 2D cultured DPCs. **(G)** Alizarin Red S staining of 2D cultured DPCs after three weeks osteogenic differentiation (scale bar is 400 μm). **(H)** Immunofluorescence images of 2D cultured DPCs using surface marker of CD90 and DAPI (scale bar is 400 μm).

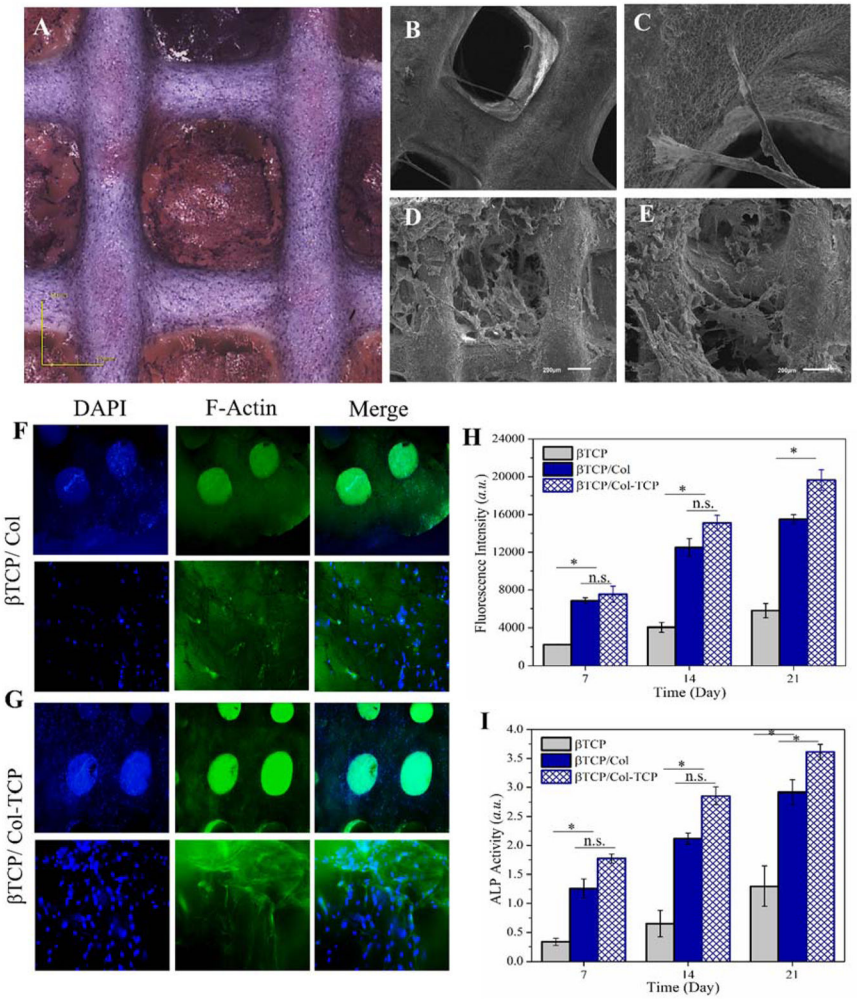

Figure 5.

(A) Hematoxylin and eosin (H&E) staining of DPCs seeded onto 3D-printed β-TCP/Col construct after three weeks. Scanning electron micrographs of **(B–C)** 3D-printed β-TCP scaffold, and **(D–E)** 3D-printed β-TCP/Col-TCP construct seeded with DPCs after three weeks (**B**, **C**: scale bar is 500 μm; **D**, **E**: scale bar is 200 μm). The immunofluorescent images of encapsulated DPCs into **(F)** β-TCP/Col, and **(G)** β-TCP/Col-TCP constructs after 3 weeks. **(H)** DPCs viability cultured onto 3D-printed β-TCP scaffold in comparison with β-TCP/Col and β-TCP/Col-TCP constructs after over three weeks. **(I)** Alkaline phosphatase (ALP) activity of DPCs cultured onto 3D-printed β-TCP scaffold in comparison with β-TCP/Col and β-TCP/Col-TCP constructs after 1, 2, and 3 weeks.